ARTICLE NO. 79-0765R

C80-030

Role of Shocks in the "Sub-Transonic" Flutter Phenomenon

20009
20018
90001

Holt Ashley*
Stanford University, Stanford, Calif.

A semi-quantitative investigation is reported on the influence of partial-chord transonic shocks on flutter of "typical-section" wing models. Unsteady airloads are assumed as the sum of linearized theory and a "shock-force doublet" centered at the measured steady shock location. The shock is shown usually to destabilize single-degree pitching motion; it may affect flexure-torsion flutter either way, often profoundly. Various typical-section parameters are studied, along with the important phase lag known to be present in the shock oscillation. Energy transfer during flutter is examined. Simplified calculations are presented that are believed relevant to the transonic tests by Farmer & Hanson.[1]

Nomenclature†

a = x_e/b, dimensionless location of elastic center or point of spring attachment
c = $2b$, airfoil chordlength (L)
C = $F+iG$, Theodorsen function[29]
C_{L_α} = lift-curve slope
C_{M_α} = slope of pitching moment curve for quarter-chord axis
C_N = section coefficient of normal force
F_i = aerodynamic functions of k, M_∞ defined by Eqs. (12-14)
G = shock function of k, M_∞ defined by Eq. (7)
i = $\sqrt{-1}$, imaginary unit
J_i = Bessel function of the first kind and order i
k = $\omega b/V$, reduced frequency
k' = modified reduced frequency, Eq. (11)
K_w = flexure spring constant (FL^{-2})
K_θ = torsion spring constant (F)
L = running lift or upward aerodynamic force (FL^{-1})
m = running mass of typical section (ML^{-1})
M_y = running nose-up pitching moment about midchord (F)
M_∞ = flight Mach number
p = static pressure (FL^{-2})
q = dynamic pressure (FL^{-2})
r_M = radius of gyration (L)
t = time (T)
T = absolute temperature
V = airspeed (LT^{-1})
V_F = critical airspeed at flutter (LT^{-1})
w = upward displacement of typical-section midchord (L)
x = chordwise coordinate, aft from midchord (L)
x_c = coordinate of mass center (L)
x_e = coordinate of elastic center (L)
x_s = steady shock location (L)
x_u = displacement of upper-surface shock from its steady location (L)
α = angle of attack of airfoil
α_{ZL} = angle of attack, measured from zero-lift attitude
γ = ratio of specific heats of a gas
θ = nose-up twist or angular displacement of typical section
λ = quantity defined by Eq. (10)
λ_i = curve-fitting parameter in Eqs. (21) and (22)
μ = $m/\pi\rho b^2$, mass ratio
ρ = ambient density of gas (ML^{-3})
χ_c = x_c/b, dimensionless c.m. location
ϕ = phase lag of simple harmonic motion
ω = circular frequency of simple harmonic motion (T^{-1})
ω_w, ω_θ = "natural frequencies" of typical section (T^{-1}), (see Table 1)
Λ = sweep angle

Subscripts, Operators, etc.

$Im\{\ \}$ = imaginary part of complex quantity
$\bar{(\ )}$ = amplitude of simple harmonic quantity
$(\ )_i$ = index used for Bessel functions, etc.
$(\ )_0$ = stagnation property of gas
$(\ )_s$ = quantity associated with shock wave
$(\ )_1$ = just ahead of shock
$(\ )_2$ = just behind shock
$(\ )_\infty$ = property of undisturbed gas
$\Delta(\ )$ = small increment

Introduction

PRIMARY flexure-torsion flutter is the most destructive of all aeroelastic instabilities and has long been recognized as a particular hazard to flight at Mach numbers near unity. Its dangers are exacerbated in that regime by a dual failure in the means used for flutter clearance. On the one hand, wind-tunnel measurements with dynamic-elastic models are expensive and may be unreliable because of wall and/or Reynolds-number effects. On the other, conventional linearized aerodynamic theory often proves hopelessly inadequate for predicting stability.

The latter failure was illustrated dramatically by the tests reported by Farmer and Hanson[1] on two models whose properties, after a small adjustment to the stiffnesses, were identical except for the distributions of profile thickness over the wing planform. Where linearized theory would foresee no difference between the two stability boundaries, the wing described as "supercritical" fluttered near Mach number M_∞ = 1.0 at dynamic pressures 25% lower than its "conventional" counterpart. The original Ref. 1 tests were con-

Presented as Paper 79-0765 at the AIAA/ASME/ASCE/AHS 20th Structures, Structural Dynamics, and Materials Conference, St. Louis, Mo., April 4-6, 1979; submitted April 20, 1979; revision received Sept. 26, 1979.

Index categories: Aeroelasticity; Transonic Flow; Nonsteady Aerodynamics.

*Professor, Aeronautics and Astronautics. Honorary Fellow AIAA.

†Dimensional quantities are identified after their definitions by the relevant combinations of L (length), T (time), M (mass), and F (force).

ducted in a Freon-12 medium at the Transonic Dynamics Tunnel, NASA Langley Research Center. More recently, air tests in the same facility[2] showed even greater differences in critical behavior.

It is the opinion of the author and others (cf. Sec. 4.2 of McGrew et al.[3]) that a predominant factor in these anomalies is the presence of shock waves located part-way back along the chords of the upper and, sometimes also, the lower wing surfaces. These shocks may move periodically in harmony with the oscillatory angle-of-attack changes and, even at very low reduced frequencies, lag significantly in phase behind what would be estimated on a quasi-steady basis. Details will be furnished below about the shocks that would clearly be present on wings like those of Ref. 1 in the M_∞ range from about 0.8 to above unity, depending on incidence. But this is not the only occasion when they have been implicated in a flutter occurrence. Shock-induced boundary-layer separation is well known to have been a cause of "aileron buzz" (e.g., Erickson and Stephenson[4]). "Shock stall" is associated with the transonic single-mode instabilities reported by Erickson.[5]

Recently, Stevenson[6] described "self-excited airfoil bending oscillations," which arose during wind-tunnel tests of a HiMAT model canard and flight tests on the B-1 wing outer panel. Motion pictures of the HiMAT incident show large changes of aerodynamic angle of attack in the unstable mode; although the author agrees with Stevenson that this was not "classical flutter," it was nevertheless a dynamic aeroelastic instability much like those described in Refs. 2 and 5. Indeed, Borland[7] has counted at least eight distinct such events which took place either in flight or during model experiments.

The investigation summarized herein is not aimed at quantitative flutter estimation for any particular lifting surface. Its goal is an inexpensive scheme for highlighting the important influence of shocks on small-amplitude flutter and for estimating the effects of various system parameters, both when the shock is present and when it is artificially removed. The term "sub-transonic" is chosen for the relevant M_∞ range because M_∞ (or $M_\infty \cos\Lambda$ on a wing of sweep angle Λ) is always appreciably less than 1.0 when part-chord shocks are active.

In this speed range the author believes that satisfactory quantitative predictions will become possible only when accurate, three-dimensional, unsteady computer codes are developed by the methods of computational fluid dynamics (CFD). It is likely, however, that several years will pass before this objective is attained.

By contrast, two-dimensional CFD tools are now at quite an advanced stage, as was forecast in the useful survey by Ballhaus[8] that is now three years old. They are just beginning to be employed in flutter claculations. The first significant instance is believed to be the study by Ballhaus and Goorjian[9] on the single-degree pitch stability of an NACA 64A006 profile near $M_\infty = 0.88$. Rizzetta[10] published a limited number of initial-condition response calculations on an NACA 64A010 typical section model, from which flutter boundaries can be inferred for a single-degree case and for a three-degree combination involving flexure, torsion and a trailing-edge flap. The aerodynamic code employed was LTRAN2 of Ballhaus and Goorjian.[11] For a fixed set of mechanical parameters and several values of mass ratio μ, his work relates not only to linear stability but demonstrates interesting nonlinear effects on motion at larger amplitudes.

The most comprehensive CFD study to date is that of Yang, et al.[12] Choosing NACA 64A006 and 64A010 typical sections, elastically restrained in flexure and torsion, they present plots of critical speed and frequency vs several system parameters. Two codes adopted are LTRAN2 and UTRANS2 of Traci, et al.[13] The trends of flutter with M_∞, μ, center-of-mass location, and flexure-torsion frequency ratio are quite similar to those found in the present investigation. Certain influences of restraining the part-chord shock motions can be inferred by comparing results based on the two codes, because UTRANS2 apparently keeps the shock position fixed. It is worth remarking that flutter calculations were also given in Ref. 13; because the shock contribution is excluded, however, there is some question whether these deserve priority over Ref. 9.

In November 1978 a workshop was organized at Columbus, Ohio, by Air Force Flight Dynamics Laboratory for the exchange of information on "Transonic Unsteady Aerodynamics for Aeroelastic Applications." Although no Proceedings will be published, considerable work in progress was described which promises to have useful consequences for flutter prediction. Notable are the programs of unsteady pressure measurement at NASA Ames and Langley Research Centers, at NLR Amsterdam and at Ohio State University. Only when a large body of such data are in hand can improved CFD code development proceed with confidence. Preliminary measurements were shown by S. Davis of Ames, for example, on an oscillating NACA 64A010 profile. They tend to verify the principle of superposition for airloads in the presence of shocks when the mean angle of attack α_{ZL} is zero, but they exhibit strong nonlinearities at $\alpha_{ZL} = 4$ deg and $M_\infty = 0.8$.

Another significant event at Columbus was the report by Ballhaus of the first successful and fully rational theoretical analysis of aileron buzz, based on a viscous CFD code such as those described in Ref. 14.

Finally, some mention must be made of the many approximate schemes that have been suggested for transonic flutter analysis of three-dimensional surfaces. One possible approach involves the "modified strip theory" of Yates.[15] It is currently being adapted[16] to the tests of Ref. 1, and one hopes that means can be found to adjust its quasi-steady features to account for such phenomena as the phase lag in shock oscillations. Garner[17] has proposed and applied a method whereby linearized theory can be corrected semiempirically through the use of measured or predicted steady pressure distributions in supercritical flow. His examples demonstrate that both the amplitude and phase lag of the shock-induced loading are estimated by this promising procedure.

The report by McGrew et al.[3] is unique in that it contains the only attempt to date at correlating with the measurements of Ref. 1—specifically on the supercritical or "TF-8A" model. Based on measured steady pressure data, "steady" and "unsteady" weighting factors are developed for application to linearized airloads obtained from a vortex-lattice method. Very careful account is taken of the model deformation under mean loading in the wind tunnel. Although the quantitative comparison of flutter dynamic pressures and frequencies is not entirely satisfactory, both weighting schemes yield the expected transonic drop in speed relative to linearized theory. The Ref. 3 conclusions on the importance of shock effects reinforce those arrived at here. Section 2.5 of Ref. 3 contains an imaginative analysis, based on nonlinear acoustics, of the supercritical flowfield and shock oscillation; it is regrettable that resource limitations did not permit the results to be incorporated more fully into the flutter calculations.

Aerodynamic Approximation

The idealization adopted herein consists of arbitrarily superimposing shock airloads upon the distributed unsteady airloads predicted by subcritical linearized theory. The selected model is guided by the summary of data and the brilliant discussion of shock motions contained in Sec. 9 of Tijdeman's thesis.[18] For estimating the stability of infinitesimal perturbations from steady state, which is the first stage of any flutter analysis, shock displacements caused by airfoil oscillations are expected to be of Tijdeman's "Type A." Reference 18 observes that important contributions to the aerodynamic lift and pitching moment result from the first-harmonic effect of the shock excursions. In the author's view there is produced a "shock-force doublet," acting close to the

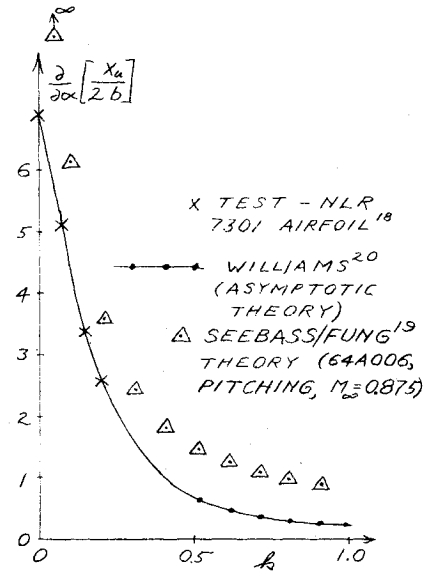

Fig. 1 Selected information on dimensionless amplitude of shock oscillation as a function of reduced frequency. Solid line defines the nominal values used here for flutter calculation.

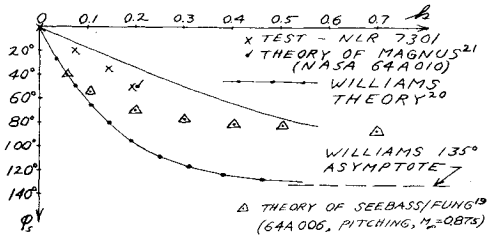

Fig. 2 Selected information on phase lag of shock oscillation as a function of reduced frequency. Solid line defines nominal values used here.

point where the steady shock meets the surface and with an amplitude proportional to the product of shock pressure jump by amplitude of shock displacement. There is a vitally important phase lag of this displacement behind the angle-of-attack changes producing it, which is believed to depend critically on the reduced frequency k.

As a first hypothesis, "universal curves" of shock amplitude and phase have been constructed vs k from data like Fig. 10.21 of Ref. 18 and the theories of Refs. 18-20. These are reproduced as Figs. 1 and 2. At a given k and Mach number M_∞, these supply complete information on the shock's effect once the steady-state strength and chordwise location are known. Since at higher k the amplitudes become small[20] as $k^{-3/2}$, the influence is greatest at the low k where most primary flutter is observed.

The term "doublet" was adopted because the incremental force due to shock oscillation reverses itself periodically while acting alternately just ahead and just behind the mean position of the shock foot. A consequence of small-perturbation theory (e.g., Williams[20]) is that, to first order in the oscillation amplitude, the shock pressure jump (p_2-p_1) can be assumed constant. It follows that four pieces of information are needed to estimate the concentrated lift and pitching moment. These are listed and discussed as follows for an upper-surface shock.

1) The amplitude x_u of the shock foot's displacement, which is assumed to be proportional to the angle-of-attack amplitude and simple harmonic in time when the latter is (cf. Fig. 10.20 of Ref. 18). Figure 1 indicates that values of the derivative $\partial(x_u/2b)/\partial\alpha$ taken from various sources are fairly consistent with one another. An exception is that small-perturbation theories predict an infinite limit as $k\to 0$. Furthermore, it has been remarked[3] that "for supercritical airfoils the shock movement versus angle of attack can be very large." Certainly that case of flat upper-surface pressure distributions near the airfoil's design point merits careful investigation. The "nominal" curve was designed to agree with NLR 7301 data at low k and with the Ref. 20 asymptote.

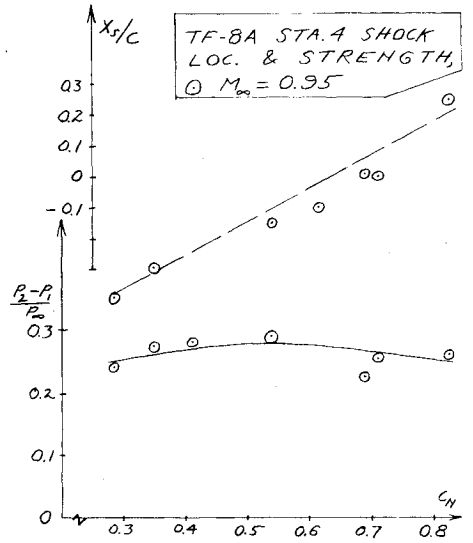

Fig. 3 Estimated chordwise location and pressure jump for upper-surface shock at flight Mach number 0.95, Sta. 4 on TF-8A wing. Data are plotted as functions of section normal force coefficient.

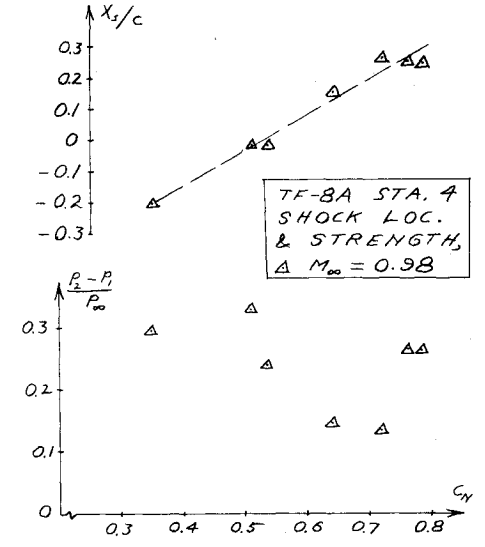

Fig. 4 TF-8A data, similar to Fig. 3, at $M_\infty = 0.98$. Pressure jump between $C_N = 0.5$ and 0.75 shows passage through "supercritical" design point.

2) The phase angle ϕ_s by which the displacement lags behind its quasi-steady behavior. Figure 2 reveals wide variations in the various estimates of this function. Had additional data been included, they would have further emphasized that ϕ_s depends not only on k but on M_∞, profile shape, angle of attack, and perhaps Reynolds number. Asymptotes at $k\to\infty$ are given by two different theories (Refs. 19 and 20, respectively) as 90 deg and 135 deg. Since many ϕ_s predictions tend substantially to exceed measured values at a given k, the nominal curve of Fig. 2 was constructed by quadrupling the abscissa scale for some results of Williams' theory. In view of this arbitrariness, it was decided to include prescribed variations in ϕ_s among the parametric studies of flutter.

3) and 4) The steady strength (p_2-p_1) and chordwise position x_s of the shock or shocks. Information on these

quantities abounds. In addition to the extensive data for NACA 64A006 and NLR 7301 profiles contained in Ref. 18 and in several predecessor reports by Tijdeman and coauthors, one can mention the following as typical sources involving two-dimensional flows: Knechtel[22] for the 9% double-wedge and 6% biconvex airfoils; and McDevitt et al.[23] for the 18% biconvex airfoil. In connection with study of the Farmer and Hanson[1] flutter tests, there is also a need for three-dimensioal data of the sort given by Montoya and Banner[24] and by Harris and Bartlett.[25] These references tabulate pressures measured, in flight and wind tunnel, respectively, on wings shaped like the supercritical model of Ref. 1. Seeking for the highest Reynolds numbers on a configuration close to that which fluttered, the author searched for shocks among the TF-8A airplane pressures reported by Ref. 24. In dimensionless form and at representative flight $M_\infty = 0.95$ and 0.98, such results appear in Figs. 3 and 4. They are given as functions of the reported section normal-force coefficient C_N at wing station 4, which was 65.3% of the distance from root to tip on the TF-8A semispan. They were calculated, initially at each actual test condition, by picking out pressure rises (through critical pressure) which were consistent with the local Mach number just ahead and with the shock-jump condition corresponding to an "effective" oblique shock angle. This angle was intended to account both for the sweepback of the shock-wing-surface intersection and for the possibility that the shock was not quite normal where it met the outer edge of the boundary layer. Because of "smearing" due to boundary-layer interaction, the pressure orifices from which p_2 and p_1 were inferred were often separated by 10–30% of the local chord. A carpet plot of strength and location vs M_∞ and C_N was prepared, from which the Figs. 3 and 4 data are interpolated. The scatter is believed due to inaccuracies in the identification process, except that at $M_\infty = 0.98$ and $C_N = 0.6$-0.7 there is a meaningful diminution in $p_2 - p_1$ due to passage close to the design point of the TF-8A wing.

Given the aforementioned quantities and the assumption of small harmonic oscillation, it is straightforward to reason that a single upper-surface shock would produce an incremental running lift and nose-up pitching moment about midchord as follows:

$$L_s = 2b(p_2 - p_1)(x_u/2b)e^{i(\omega t - \phi_s)} \tag{1}$$

$$M_{y_s} = -4b^2(x_s/2b)(p_2 - p_1)(x_u/2b)e^{i(\omega t - \phi_s)} \tag{2}$$

Note that $2b$ and c are used interchangeably for wing chord, there being no agreed notation in the field of aeroelasticity. Reduced frequency k is always based on b in this paper. Real parts of complex quantities are to be taken in the usual way. If there were also a lower-surface shock, its contribution could be added to Eqs. (1) and (2) in an obvious fashion. In particular, for a symmetrical profile at zero incidence, the two shock contributions reinforce and require a factor of 2 to be applied to L_s and M_{y_s}.

Figure 5 shows that the generalized coordinates adopted for flexure-torsion flutter calculations are the upward displacement $w(t)$ at midchord and the twist $\theta(t)$ about this axis. At the low k considered here, it is an adequate approximation (cf. the small-disturbance CFD analyses of Refs. 11 and 19) to use

$$\Delta\alpha(t) = \theta - \dot{w}/V \tag{3}$$

as the angle of attack effective for determining shock displacement. Thus

$$\frac{x_u}{2b}e^{i\omega t} \cong \frac{\partial}{\partial\alpha}\left(\frac{x_u}{2b}\right)\left[\bar{\theta} - ik\frac{\bar{w}}{b}\right]e^{i\omega t} \tag{4}$$

where the overbar identifies the complex amplitude of a simple harmonic quantity.

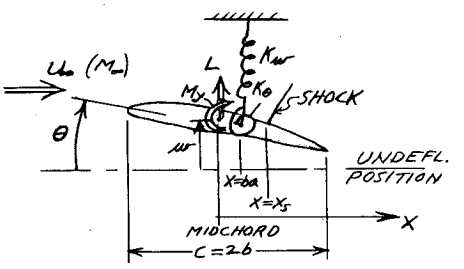

Fig. 5 The "typical section" flutter model, defining certain quantities used in the present paper.

When Eq. (4) is substituted into Eqs. (1) and (2), it proves convenient to introduce the following dimensionless notation:

$$L_s = \pi\rho V^2 b[\bar{\theta} - ik(\bar{w}/b)]e^{i\omega t}G(k,M_\infty) \tag{5}$$

$$M_{y_s} = -2\pi\rho V^2 b^2[\bar{\theta} - ik(\bar{w}/b)](x_s/2b)e^{i\omega t}G(k,M_\infty) \tag{6}$$

where

$$G(k,M_\infty) \equiv \frac{2}{\pi\gamma M_\infty^2}\left[\frac{p_2 - p_1}{p_\infty}\right]\frac{\partial}{\partial\alpha}\left(\frac{x_u}{2b}\right)e^{-i\phi_s} \tag{7}$$

Note that the last two factors in Eq. (7) are functions of k only, in view of the approximations underlying Figs. 1 and 2, whereas the rest depends strictly on M_∞ for a given profile, incidence and Reynolds number.

As approximations to the disturbed airloads due to the oscillation, the low-k theory of Kemp and Homicz[26] was selected in preference to several other alternatives. When compared with exact subsonic linearized theory, their results combine satisfactory accuracy with explicit formulas more readily adaptable to fast machine computation. Without giving all details, it is asserted that the following expressions can be derived for the flexure-torsion oscillation:

$$L = \pi\rho V^2 b\{[\bar{\theta} - ik(\bar{w}/b)]F_1(k,M_\infty) + ik\bar{\theta}F_2(k,M_\infty)\}e^{i\omega t} \tag{8}$$

$$M_y = \pi\rho V^2 b^2\{[\bar{\theta} - ik(\bar{w}/b)]F_2(k,M_\infty) + ik\bar{\theta}F_3(k,M_\infty)\}e^{i\omega t} \tag{9}$$

The three functions F_i here contain the familiar Bessel function J_0, J_1, and J_2 of the argument

$$\lambda \equiv \left(\frac{k}{1 - M_\infty^2}\right)\left\{M_\infty^2 - \sqrt{1 - M_\infty^2}\,\ell n\left[\frac{1 + \sqrt{1 - M_\infty^2}}{M_\infty}\right] - \ell n\left(\frac{M_\infty}{2}\right)\right\} \tag{10}$$

There also appears the Theodorsen function C of classical unsteady airfoil theory (cf. Sec. 5-6 of Ref. 27), with argument

$$k' \equiv k/(1 - M_\infty^2) \tag{11}$$

Specifically,

$$F_1(k,M) = (2/\sqrt{1 - M_\infty^2}) < [J_0 - iJ_1]\{C(k')[J_0 iJ_1] + iJ_1\} + (i(k' - \lambda)/2)\{J_0[J_0 - J_2] + 2J_1^2\} > \tag{12}$$

$$F_2(k,M_\infty) = (1/\sqrt{1 - M_\infty^2}) < iJ_1[J_0 - J_2] + [J_0 - iJ_1]C(k')[J_0 - J_2 - 2iJ_1] + \left[1 - \frac{k'}{\lambda}\right]J_0 J_2 + \left[1 + \frac{k'}{\lambda}\right]J_1^2 > \tag{13}$$

$$F_3(k,M_\infty) = \frac{1}{\sqrt{1-M_\infty^2}} < \frac{1}{2}\,[J_0 - J_2 - 2iJ_1]\{C(k')\,[J_0 - J_2 - 2iJ_1] - [J_0 - J_2]\} - i\left\{\left(\frac{k'-\lambda}{3}\right)J_0^2 + \left[\frac{4-k'}{3\lambda^2} + \frac{2(k'-\lambda)}{3}\right]J_1^2 - \left[\frac{k'}{\lambda^2} + \frac{k'-\lambda}{3}\right]J_0 J_2\right\} > \quad (14)$$

It was the Kemp and Homicz[26] choice of the midchord axis for pitching moment M_y that influenced the selection of coordinates w and θ here. Equations (8, 9, 12, 13, and 14) are stated to be correct up through 0 ($kM_\infty/(1-M_\infty^2)$) and "remarkably accurate" when this parameter equals $\pi/4$. Since Mach numbers fairly close to unity are encountered in the present investigation, a further check was conducted by comparison with the eight aerodynamic derivatives from Table W3 of Van der Vooren.[28] Corresponding Ref. 26 quantities were computed at M_∞ = 0, 0.5, 0.6, 0.7, and 0.8 (the highest value tabulated in Ref. 28) and for k between 0 and 0.2. As expected, the agreement is exact in incompressible flow. Up through M_∞ = 0.7 all comparisons are within ±5% except for a couple of very small derivatives like the out-of-phase moment due to plunge oscillation. Errors >10% are encountered at M_∞ = 0.8 and k = 0.2, but this is perhaps to be expected since $k' \cong 0.55$.

Typical Section Equations of Motion

With the elastic center (point of attachment of restraining springs) located at $x = x_e$, chordwise mass center at $x = x_c$ and other parameters as illustrated on Fig. 5, the equations of motion for the typical section flutter model of unit span read

$$m\ddot{w} + K_w w - mx_c\ddot{\theta} - K_w x_e\theta = L_s + L \quad (15)$$

$$-mx_c\ddot{w} - K_w x_e w + (mr_M^2)\ddot{\theta} + [K_\theta + K_w x_e^2]\theta = M_{y_s} + M_y \quad (16)$$

Here m is the running mass, r_M is radius of gyration about midchord, and the lifts and moments are given for simple harmonic motion by Eqs. (5-14). This system is the one originally devised by Theodorsen[29] for flutter studies in incompressible flow; relations between the present symbols and those used in Ref. 29 are tabulated in Table 1. For convenience in applying the aerodynamic theory of Ref. 26, the parameters used to describe the typical section differ in some respects from those originally defined in the work of Theodorsen and its extension by Garrick.[32] Table 1 shows how the quantities in their papers can be calculated in terms of similar quantities defined here.

The author was tempted to work with arbitrary time-dependent motion and therefore characterize stability by the root-locus technique, which is (happily) now making a wider appearance in the aeroelastic literature. Since the intention is to examine the influence of system parameters, however, it seems more efficient to assume sinusoidal oscillation and present the results as stability boundaries. Taking ω to be the flutter frequency and other dimensionless quantities as defined in Table 1, one easily manipulates Eqs. (15) and (16) into the following algebraic relations involving the complex amplitudes w/b and θ:

$$\left\{\frac{(\omega_w/\omega_\theta)^2}{(\omega/\omega_\theta)^2} - 1 + \frac{i}{\mu k}\,[F_1 + G]\right\}\frac{\bar{w}}{b} + \left\{\frac{a(\omega_w/\omega_\theta)^2}{(\omega/\omega_\theta)^2} - \chi_c + \frac{1}{\mu k^2}\,[F_1 + G + ikF_2]\right\}\bar{\theta} = 0 \quad (17)$$

Table 1 Relation between symbols in Ref. 32 and the present paper

Theodorsen	Present investigation
α	$=\theta$
h	$=-(w-ba\theta)$
a	$=a$
x_α	$=(\chi_c - a)$
r_α^2	$=\rho_M^2 + a(a-2\chi_c)$
κ	$=1/\mu$
k	$=k\,(\equiv \omega b/V)$
ω_h^2	$=\omega_w^2$
ω_α^2	$=\omega_\theta^2\left\{\dfrac{1 + \dfrac{a[2\chi_c - a]}{\rho_M^2 - a[2\chi_c - a]}}{1 + a^2\dfrac{K_\omega b^2}{K_\theta}}\right\}$

$$\left\{\frac{\chi_c}{\rho_M^2} - \frac{a}{\rho_M^2}\frac{(\omega_w/\omega_\theta)^2}{(\omega/\omega_\theta)^2} + \frac{i}{\mu k\rho_M^2}\left[F_2 - \frac{x_s}{b}G\right]\right\}\frac{\bar{w}}{b} + \left\{\frac{1}{(\omega/\omega_\theta)^2} - 1 - \frac{1}{\mu k^2\rho_M^2}\left[F_2 - \frac{x_s}{b}G + ikF_3\right]\right\}\bar{\theta} = 0 \quad (18)$$

Neutral stability is associated with vanishing of the characteristic determinant of Eqs. (17) and (18). For prescribed values of M_∞, k, and all but two of the other parameters, explicit solution generally yields a pair of flutter points. Details of particular cases are given in what follows.

Single Degree-of-Freedom Instability

Although not so representative of "real-world" problems as the flexure-torsion case, single-degree pitching flutter of the airfoil constitutes a simple example that helps to explain the effects of "sub-transonic" shocks. After a flurry of incompressible-flow studies in the late 1940's, Runyan[30] published a definitive investigation of this phenomenon, which included linearized-theory calculations at subsonic M_∞ = 0.5 and 0.7. The situation can be analyzed with Eqs. (15) and (16) by introducing a frictionless pivot at $x = ba$ so that the coordinates are related by

$$w(t) = ba\theta(t) \quad (19)$$

The torsion spring K_θ is attached at the pivot. A single equation of rotational motion is then derived by transferring the aerodynamic moment $[M_{y_s} + M_y]$ to the new axis by adding $b\,a\,[L_s + L]$.

With simple harmonic pitching assumed, a necessary condition[30] for neutral stability is that the out-of-phase component of the moment must vanish, that is, no aerodynamic work is done on the oscillation. In dimensionless terms, this condition reads

$$-Im\left\{\sqrt{1-M_\infty^2}\,[1 - ika]\left[\frac{x_s}{b} - a\right]2G(k,M_\infty)\right\} + \{[J_0 - J_2]\,[J_0 G(k') - J_1 F(k')] + J_1[J_0 - J_2] - 2J_1[J_0 F(k') - J_1 G(k')]\} + k\left\{\frac{-(J_0 - J_2)^2}{2} + 2J_1[J_0 - J_2]G(k') + \left[\frac{(J_0 - J_2)^2}{2} - 2J_1^2\right]F(k')\right\}$$

$$+2a\left\{\left[\frac{k'-\lambda}{2}\right][J_0^2-J_0J_2+2J_1^2]+J_0J_1\right.$$
$$\left.+[J_0^2-J_1^2]G(k')-2J_0J_1F(k')\right\}$$
$$-2ka^2\{J_1^2+[J_0^2-J_1^2]F(k')+2J_0J_1G(k')\}=0 \qquad (20)$$

In Eq. (20), the first term is the shock contribution, here written with a factor of two for the symmetrical profile at $\alpha_{ZL} = 0$. Other symbols have appeared previously except for $F(k')$ and $G(k')$, which are the real and imaginary parts of $C(k')$. Given that Eq. (20) is satisfied, a sufficient condition[30] for neutral stability, relating the inertial and elastic properties, is furnished by the in-phase terms of the moment equation. The latter is not considered further here, because the shocks' role is best highlighted by examining the energy transfer.

To begin with, a check on the potential-theory approximation can be made by dropping the shock term from Eq. (20) and comparing the roots with Runyan's calculations. Figure 6 is a tracing of Fig. 4 from Ref. 30, whereon the necessary condition at three subsonic Mach numbers is plotted in terms of dimensionless pitch-axis location a vs inverse reduced frequency. At their lower asymptotes, all the curves approach the quarter-chord line $a = -0.5$, behind which subsonic stability always seems to be positive. The dashed curves reflect the theory of Ref. 26. As expected, agreement is perfect at $M_\infty = 0$; and it is always satisfactory on the lower branch and in the "nose" regions near maximum k. Surprisingly, the branches of the two sets of curves involving far forward axis locations are seen to diverge at $M_\infty = 0.5$ and 0.7, even though the Ref. 26 approximation should be excellent as $k \to 0$. Close examination of the moment expressions indicates an extreme sensitivity of the stability boundary in this region to small inaccuracies in the computations. The disagreement is, therefore, attributed to round-off error, and one cannot say whether the solid or dashed curves are closest to the truth; the author[31] of Ref. 30 concurs in this conclusion.

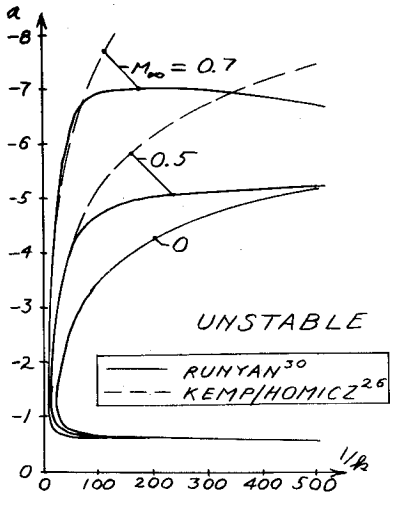

Fig. 6 Necessary condition for single-degree pitch instability, shown as a stability boundary of pitch axis location vs inverse reduced frequency.

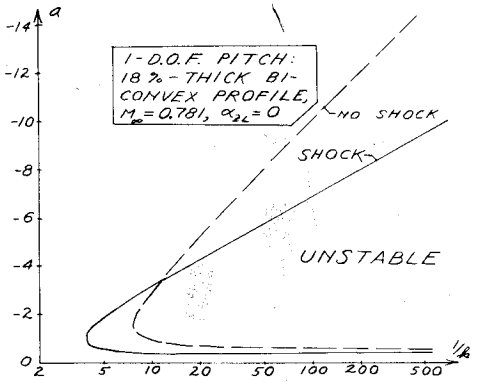

Fig. 7 Shock's effect on the single-degree pitch necessary stability boundary for an 18%-thick biconvex airfoil at $M_\infty = 0.781$.

Many stability boundaries, with and without the shock term, have been calculated from Eq. (20). The most pronounced shock effect was found on the 18%-thick biconvex profile (data from Ref. 23), and an example for $M_\infty = 0.781$ is given in Fig. 7. The logarithmic $1/k$ scale is adopted to emphasize the destabilizing effect near the nose, which is where such an instability is most likely to be encountered in practice. Figure 8 expands upon the comparison, showing how the nose locations (or maximum possible reduced frequencies at which instability can occur) vary with M_∞; the range here is between first shock appearance around $M_\infty = 0.7$ and where shock-induced separation invalidates the model.

One discovers in the phase angle ϕ_s a mechanism to explain these predictions. For axis locations near the leading edge at $a = -1$, the angle of attack which controls the shock displacement at low k is θ. Since the quasi-steady effect of M_{y_s} resembles a restoring spring on θ, any lag in the restoring moment feeds energy into the oscillation, giving rise to an increased area of instability relative to potential theory. As a becomes more negative the contribution of the plunging degree of freedom $w(t)$ to the shock motion [Eq. (19)] begins to predominate over pitch. For plunging, ϕ_s must exceed 90 deg before the airstream can feed in energy, and Fig. 2 shows this is impossible in the k range of interest.

Incidentally, calculations similar to the foregoing were conducted in search of "pure" plunging instability. The shocks' influence proved to be stabilizing at all k and M_∞ where their airload contribution was significant. Thus the author's view is confirmed that some pitching motion must occur even in "single-degree" cases such as those of Ref. 6.

Flexure-Torsion Flutter

Several tens of thousands of flutter points have been obtained from Eqs. (17) and (18), with and without the terms containing $G(k,M_\infty)$. After expansion of the flutter determinant, one discovers that vanishing of its imaginary part provides a linear relation between $1/\mu$ and the frequency-ratio parameter $(\omega_\theta/\omega)^2$. A convenient calculation procedure, therefore, consists of prescribing M_∞, k, and the remaining parameters a, χ_c, $\rho_M{}^2$, and ω_w/ω_θ. Solving the imaginary equation for $(\omega_\theta/\omega)^2$, one substitutes the result into the real equation, which becomes a quadratic in μ. Solution of the

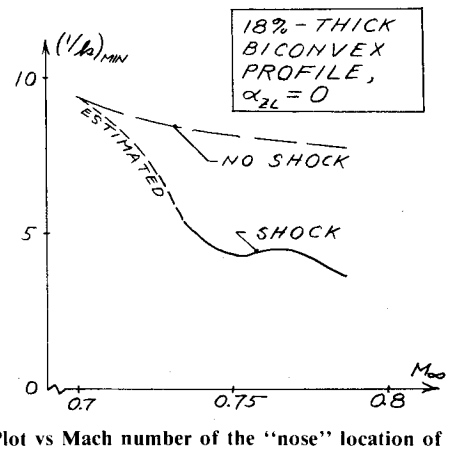

Fig. 8 Plot vs Mach number of the "nose" location of curves like Fig. 7 showing the shock's large influence in this region.

latter yields two pairs of eigenvalues. Flutter roots are then readily found in terms of $V_F/b\omega_\theta$ and ω/ω_θ. For brevity, only flutter speeds are presented in the graphs that follow. Each is, of course, accompanied by a frequency. No surprises appeared in the latter, the trends being similar to earlier subcritical-flow results (e.g., Garrick[32]). The shock influences on frequency are of the same general magnitudes as those on speed.

As an initial check of the computer program, cases were run at $M_\infty = 0.7$, with $G(k,M_\infty) = 0$, and set alongside corresponding data at the lower k from Table III of Garrick.[32] Because of small differences in the definitions of some system parameters, no precisely analogous pairs of eigenvalues were obtained. But where the properties were close to one another, the predicted speeds and frequencies compared within ±10%.

Figures 9-13 are representative of the trends shown by calculations designed to illustrate shock effects. They all refer to the 64A006 profile ("Type A" shock data from Ref. 18) at $\alpha_{ZL} = 0$ and for the other dimensionless quantities listed in the boxes.

The Figs. 9 and 10 curves can be interpreted as indicating roughly how flutter speed varies with altitude for a given wing, since μ is inversely proportional to ambient density. For frequency ratio $(\omega_w/\omega_\theta) = \sqrt{0.1}$ Fig. 9 shows that adding the shock contribution onto the distributed airloads is markedly favorable over the whole μ range covered. A contrasting situation arises (Fig. 10) when the frequency ratio is increased to unity and M_∞ reduced by only 0.02. Here logarithmic scales are adopted so as to permit careful detailing of how the speed goes off to infinity as μ drops from 10 to about 4; small wiggles in the curves are believed to reflect accurate calculations. In this case one observes that both the degree and the direction of the shocks' effect depend very much on where one looks along the μ scale.

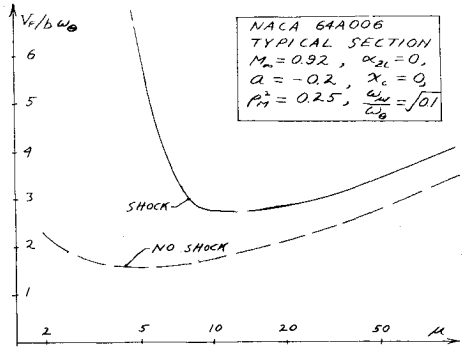

Fig. 9 Shock's effect on dimensionless flutter vs speed mass ratio for the NACA 64A006 "typical section" with the listed parameters.

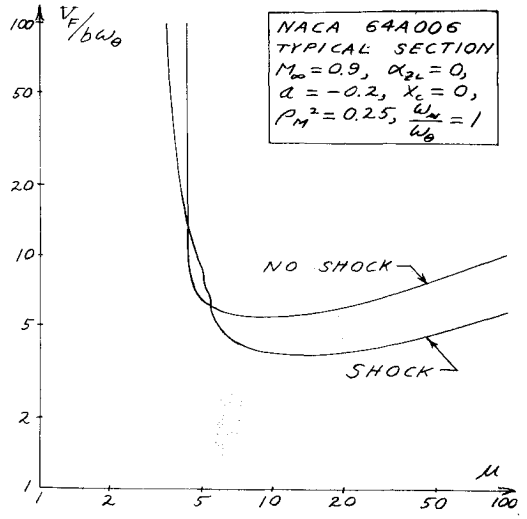

Fig. 10 Plot similar to Fig. 9, except that $M_\infty = 0.9$ and bending-torsion frequency ratio is increased from $\sqrt{0.1}$ to 1.0.

Cross plots vs μ at five values of ω_w/ω_θ and ten values of center-of-mass location χ_c were used to construct the curves of Figs. 11 and 12. For $\mu = 50$, which is typical of a high-performance aircraft flying in the lower atmosphere, Fig. 11 depicts circumstances where adding the shock causes nearly a 50% reduction in $V_F/b\omega_\theta$ at frequency ratios above unity. Other studies based on linearized theory (see, e.g., figures in Chap. 9 of Ref. 27) often show a pronounced flutter-speed minimum near $(\omega_w/\omega_\theta) = 1$. The case selected here, however, involves no such "resonance" but rather a dimunition of the shock influence and leveling off of the curves below 0.5.

At $\mu = 25$, 50, and a low (ω_w/ω_θ), Fig. 12 reveals the familiar unfavorable flutter tendency of moving the c.m. aft while holding a fixed elastic center. Again the difference between the shock and no-shock behavior is diminished as χ_c increases.

It is well known that a simple physical explanation is usually impossible for the instability of a multi-degree-of-freedom system. Nevertheless, qualitative attempts were made to understand the shocks' role in flexure-torsion flutter by close examination of the mode shapes in a number of examples. The hope was that at least some instances might be discovered where the motion at flutter was equivalent to oscillation about a nearly fixed chordwise axis location—whereupon the energy transfer mechanism might resemble that in the single-degree pitch instability. Curiously, the phase angle between $w(t)$ and $\theta(t)$ turns out nearly always to be such that no "effective axis" can be identified.

In another effort at physical understanding, the energy transfer was computed directly from the lifts, moments, and mode shape. The total aerodynamic work per cycle of oscillation at flutter must, of course, be zero. But this work can be separated into a portion from the shock and a cancelling portion from the linearized-theory airloads. Consider two points taken from Fig. 10. For $\mu \cong 4.72$ it is found that the work per cycle done on the flutter by the shock-force doublet (as a fraction of the mean kinetic energy of the oscillation) is

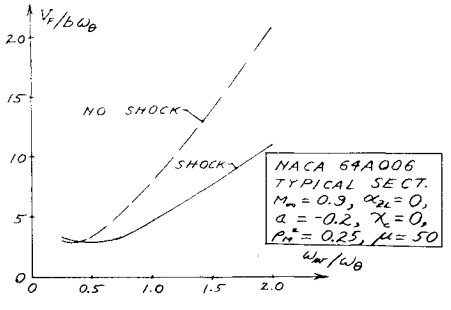

Fig. 11 Dimensionless flutter speed, with and without shocks, plotted vs frequency ratio for the NACA 64A006 "typical section" at $\mu = 50$ and other parameters as listed.

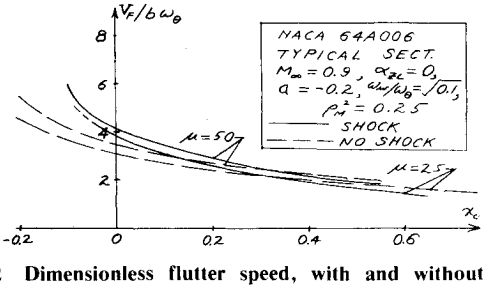

Fig. 12 Dimensionless flutter speed, with and without shocks, plotted vs center-of-mass location for the NACA 64A006 "typical section" at $\mu = 25$, 50, and other parameters as listed.

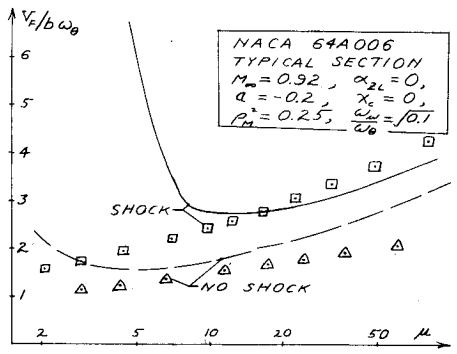

Fig. 13 Data of Fig. 9, compared with parallel calculations with aerodynamic derivatives supplied by Seebass & Fung. In the latter, all phase lags have been arbitrarily reduced by 50%.

-0.469, clearly a strong "favorable" effect. At $\mu \cong 25$, by contrast, the same parameter has a value + 1.350 and helps to explain a decrease in $V_F/b\omega_\theta$ from 6.41 to 4.02.

During the course of studies on the 64A006 typical section and on the model described below as the "TF-8A," a useful exchange of correspondence took place with C.R. Seebass and his collaborators (authors of Refs. 19 and 33 and other papers on small-perturbation transonic CFD). Among other information, they kindly supplied the author with curve-fits for their CFD predictions of the lift, quarter-chord pitching moment, and shock displacement due to pitching oscillation of the 64A006 at $\alpha_{ZL}=0$ and $M_\infty = 0.875$. With notation related to that of the present paper, these results can be written in the following matrix form:

$$\begin{Bmatrix} C_{L_\alpha}(t) \\ (C_{M_\alpha}(t))_{c/4} \\ \dfrac{x_{u_\alpha}(t)}{2b} \end{Bmatrix} \cong \begin{Bmatrix} C_{L_{\alpha_0}} \\ C_{M_{\alpha_0}} \\ \dfrac{\partial}{\partial\alpha}\left(\dfrac{x_u}{2b}\right)_0 \end{Bmatrix} \frac{e^{i(\omega t-\phi_i)}}{\sqrt{1+(2k/\lambda_i)^2}} \quad (21)$$

In Eq. (21) the phase lags are

$$\phi_i = \sin^{-1}\left[\frac{(2k/\lambda_i)}{\sqrt{1+(2k/\lambda_i)^2}}\right] \quad (22)$$

With index i cycled through L (lift), M (moment) and s (shock), the amplitude quantities and values of the curve-fitting parameter λ_i are

$$C_{L_{\alpha_0}} = 23.6 \qquad \lambda_L = 0.084$$

$$C_{M_{\alpha_0}} = -4.45 \qquad \lambda_M = 0.069$$

$$\frac{\partial}{\partial\alpha}\left(\frac{x_a}{2b}\right)_0 = 10.9 \qquad \lambda_s = 0.067$$

The lift and moment here contain contributions from both distributed airloads and the shock-force doublet. A revealing measure of the latter's importance is that the Prandtl-Glauert rule yields a steady lift-curve slope of 13 at $M_\infty = 0.875$; when compared to 23.6, this proves the shock to be responsible for almost half the incremental lift.

Without full details, it is yet obvious that Eqs. (21) and (22) offer the possibility of very simple flutter calculations when inserted into Eqs. (15) and (16). This has been carried out in a few cases, both with the complete formulas and with the shock terms removed by subtracting expressions similar to those for L_s and M_{y_s}. From Fig. 4 of Fung et al.,[33] it was inferred that the corresponding steady-state shock data are $(x_s/2b) = 0.21$ and $(p_2-p_1)/p_\infty = 0.348$. These values fall closest to those used here for $M_\infty = 0.92$ in Fig. 9, so the most meaningful comparison can be made at that Mach number.

Unfortunately, the first set of flutter eigenvalues based on Eqs. (21) and (22) bore little resemblance to Fig. 9. In recognition that the phase lags from Eq. (22) are much larger than those assumed here, experiments were conducted with arbitrary reductions to all three ϕ_i. Considerably better agreement was then found, of which the points shown as squares and triangles on Fig. 13 furnish a favorable example. These points relate to the "shock" and "no-shock" cases, respectively, where a factor of ½ has been applied to all angles computed from Eq. (22). The comparison with the present simplified theory is encouraging in the higher range of μ's.

An obvious conclusion is that more research must be devoted to learning why phase lags computed by certain CFD codes are so much larger than observed in tests like those of Ref. 18.

TF-8A Flutter Model

Figures 14–20 summarize efforts to introduce steady angle of attack and airfoil camber effects into the investigation. The chosen model is called "TF-8A" because its typical-section properties are taken from the 65.3% semispan station on the "supercritical" wing of Ref. 1. As discussed in connection with Figs. 3 and 4, this station is one where shock data are deducible from the Refs. 24 and 25 pressure measurements. Only upper-surface shocks are involved in the cases analyzed.

Because almost pure uncoupled bending and torsion shapes are involved, respectively, the circular frequencies ω_w and ω_θ are assumed to equal those for the second cantilever bending and torsion modes reported in Ref. 1. These and other data, as accurately as they can be inferred from Ref. 1 and curves and tables in Ref. 3, are as follows‡:

$$(\omega_w/2\pi) = 18.08\text{s}^{-1} \qquad (\omega_\theta/2\pi) = 37.10\text{s}^{-1}$$

$$(\omega_w/\omega_\theta)^2 = 0.2375 \qquad a = 0$$

$$\chi_c = 0.268 \qquad \rho_M{}^2 = 0.1921$$

The range of mass ratio reflected in the higher transonic flutter points of Ref. 1 is estimated at $\mu = 55$ to $100+$.

Characterization of the unit-span typical section is completed by explaining that a cut was taken normal to the 50% chordline, whose outboard sweep angle is $\Lambda = 40.15$ deg. The effective chord is then the streamwise chord multiplied by $\cos\Lambda$, which leads to $b = .1704$ m. The running mass is $m = 3.71$ Kg/m.

A simple-sweep aerodynamic approximation was adopted. Thus the values of Mach number used in the two-dimensional flutter solutions are $M_\infty \cos\Lambda$, with $M_\infty = 0.5$, 0.8, 0.89, 0.95, and 0.98. Normal force coefficients C_N given in the figures correspond to the section values of C_N for which upper-surface shock data were calculated from Ref. 24. No shocks are present at $M_\infty = 0.5$ or at the arbitrarily specified $C_N = 0$. The lowest C_N reported in flight at the 65.3% station is around 0.25; it is worth noting that, in order to avoid overloads on the model and to maintain a prescribed twist, the wind-tunnel C_N from Ref. 1 are lower than this.

Figure 14 presents "no-shock" plots of $V_F/b\omega_\theta$ vs μ at three Mach numbers, obtained from Eqs. (17) and (18), with $G(k,M_\infty)=0$, in the manner described above. Special attention is given to the nose and turnback of the curve for $M_\infty = 0.98$, but nearly all of these and subsequent curves present a similar behavior (not shown in detail) near their low μ ends. At μ's above 10-20 the general proportionality of V_F to $\sqrt{\mu}$, familiar from older subsonic studies,[27] is again observed.

‡From personal communication, there is some question whether the sign of χ_c should be + or −. Number here is from Fig. 3-1.5, Ref. 3.

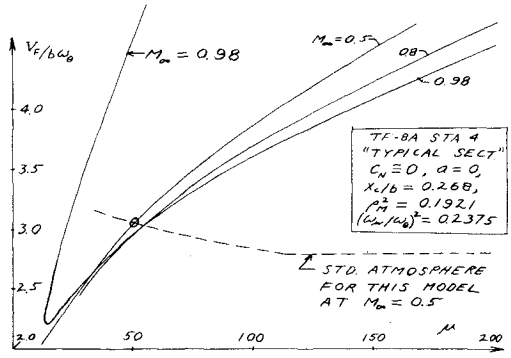

Fig. 14 Plots of dimensionless flutter speed vs mass ratio for the TF-8A model at three flight Mach numbers, with shock effects absent. To illustrate determination of a "matched point" (circled), the dashed curve shows how $V_F/b\omega_\theta$ would vary with μ in the standard atmosphere at $M_\infty = 0.5$.

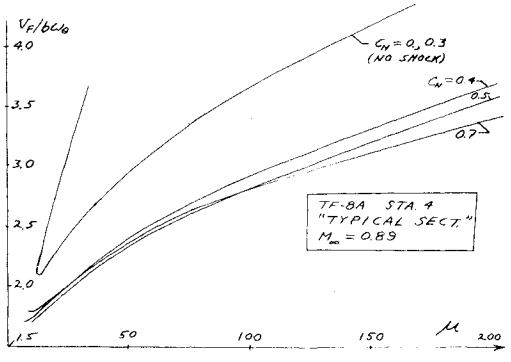

Fig. 15 Influence of section normal force coefficient on TF-8A flutter curves at $M_\infty = 0.89$.

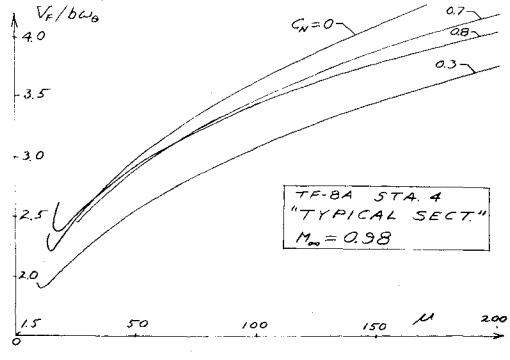

Fig. 16 Plots similar to Fig. 15 except at $M_\infty = 0.98$, which is close to the design point for the TF-8A wing.

The line marked "STD. ATMOSPHERE" illustrates how a so-called "matched point" might be determined for this model. Given that $M_\infty = 0.5$, $b\omega_\theta = 40.2$ m/s and $(m/\pi b^2) = 40.1$ kg/m^3, one can start with the variation of sound speed vs density in the standard atmosphere and construct the dashed curve of $V/b\omega_\theta$ vs μ. (The horizontal, straight-line portion corresponds to constant speed in the stratosphere.) The dashed curve then intersects the solid line for $M_\infty = 0.5$ at an actual flutter condition. For even lower altitudes and $M_\infty = 0.5$ the model is theoretically unstable. This model was, incidentally, designed for testing at quite small ambient densities. As a consequence, the matched points at higher M_∞ all occur well up in the stratosphere.

Figures 15 and 16 exemplify the influences of C_N, or angle-of-attack, changes on flutter. It bears repeating that such predictions are beyond the capability of wholly linearized

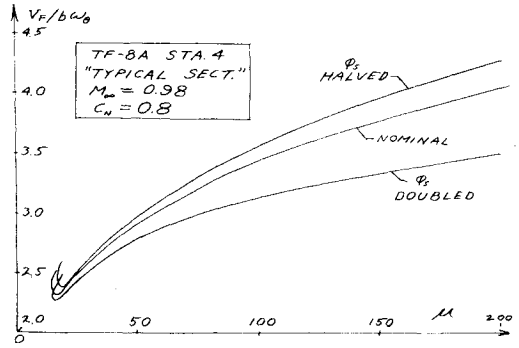

Fig. 17 Effect of arbitrary changes in shock phase lag on the TF-8A flutter curves at $M_\infty = 0.98$ and C_N.

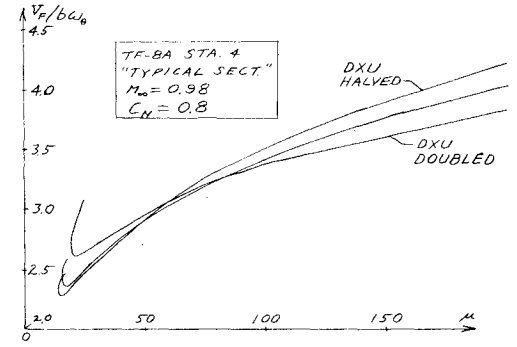

Fig. 18 Plots similar to Fig. 17, except that arbitrary changes are made in amplitude of shock displacement.

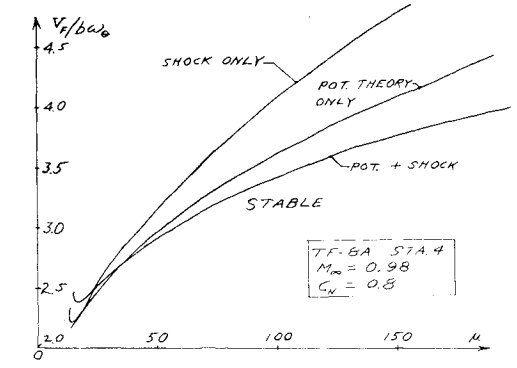

Fig. 19 Flutter curves for the TF-8A model at $M_\infty = 0.98$ and $C_N = 0.8$ calculated by means of the three indicated aerodynamic approximations.

aerodynamics. For $M_\infty = 0.89$, data like Fig. 3 reveal a progressive rearward movement with increasing C_N by a shock of nearly constant strength. Figure 15 shows that, with the specified system parameters, such movement is destabilizing for flutter. By contrast (study Fig. 4), there is a region of higher $V_F/b\omega_\theta$ around $C_N = 0.7$ at $M_\infty = 0.98$. This is precisely the design-point region for the TF-8A wing, and the local dimunition of shock strength is favorable for flutter. In view of the small size of this area in $C_N - M_\infty$ space, however, one concludes that it would be very unwise to base any flutter clearance on tests or calculations conducted near the design point of a supercritical configuration.

In Figs. 17 and 18 one sees a sample of the analyses intended to demonstrate how the critical speed is affected by arbitrary factors applied to the phase-lag and amplitude parameters from Figs. 2 and 1, respectively. In this case, but not always, an increase of ϕ_s is destabilizing. It is a fairly general conclusion that critical conditions are more sensitive to phase than to shock-amplitude variations.

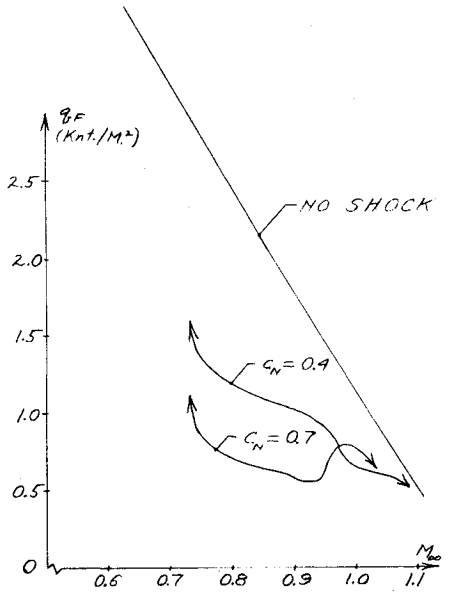

Fig. 20 Shock's influence (as applied by changing C_N) on matched flutter points for the TF-8A model in a transonic wind tunnel. Stagnation pressure and Mach number are the quantities being varied, with stagnation temperature held at 322 K.

Figure 19 exemplifies a rather inconclusive study intended to determine whether the shock could, by itself, be responsible for instability. This was suggested by Figs. 10.8 and 10.9 of Tijdeman,[18] which show instances where the distributed pressures seem to contribute much less than the shock to the resultant airloads. One notes that dropping the potential theory terms from the determinant can yield a flutter curve of the same shape and general location as those computed by two prior aerodynamic hypotheses. It must be admitted, however, that other cases could be presented where the correlation is not nearly as reasonable as in Fig. 19. For example, the "pure-shock" flutter speed behaves very anomalously in the parameter range where the steady shock location x_s passes through the section c.m.

Another way in which the TF-8A calculations can be used is illustrated by Fig. 20. Match-point curves are shown there for three angles of attack, which try to simulate testing in a facility like the NASA Transonic Dynamics Tunnel. Flutter points are sought by changing the tunnel Mach number and/or stagnation pressure p_0 while holding stagnation temperature (here assumed T_0 = 322 K) nearly constant. Take the latter procedure as an example: with M_∞ fixed, it is an easy matter for a given model to construct a plot of $V/b\omega_\theta$ vs μ. Placing it on a diagram like those in Figs. 14–19, one picks the flutter point by finding the intersection with a $V_F/b\omega_\theta$ curve corresponding to the same M_∞. With p_0 and M_∞ given, an isentropic-expansion formula then yields the flutter dynamic pressure

$$q_F = (\gamma/2)p_\infty M_\infty{}^2 \tag{23}$$

When match-point calculations are conducted for several M_∞ and $C_N = 0$, 0.4, and 0.7, the Fig. 20 curves of flutter dynamic pressure are the result. Shock data are available only in the range $M_\infty = 0.8$–0.98, so arrows are placed on the lower curves to suggest that they must merge smoothly with the "no-shock" curve. At the low end of the M_∞ scale this would occur just above critical M_∞, where the shock disappears: at the high end, it is where the shock passes off the trailing edge.

It is not claimed that any part of Fig. 20 bears more than a qualitative relationship to the Ref. 1 flutter boundary for the TF-8A wing. The C_N here are higher than the $C_N = 0.1$–0.2 of Ref. 1, for which there are no flight data on shocks. None of the curves turn sharply back to higher q_F, as they should when M_∞ exceeds unity. And, of course, the aerodynamic and structural approximations are quite unacceptable for a serious flutter analysis.

Interesting, however, is the way in which dynamic pressure is forced downward to very low values due to the shock's presence. For the assumed working gas (air), most matched points fall at reduced frequencies around 0.06 and μ in the range 600–3000. Under these circumstances, as one might infer from Figs. 15 or 16, the absolute differences in flutter speed due to changes in C_N are very large. One also expects the instabilities to be rather mild, since q is so low. This hypothesis helps to explain the difficulty Farmer and Hanson[1] had in distinguishing true flutter from motion with "low damping," even in Freon-12 where ρ_∞ is higher.

A further observation also relates to the medium in Fig. 20 being air, whereas the published tests were in Freon-12 at $\gamma = 1.12$. Although significant, the effect of changing from one gas to the other is not thought to be large. For instance, Seebass[34] remarks that one such effect is an 11½% reduction in the factor $(\gamma + 1)$ which appears in theoretical expressions for the shock-amplitude derivative, while ϕ_s is believed to be unaltered.

Concluding Remarks

This paper proposes and applies a simple, but not unrealistic, scheme for introducing the effects of part-chord shock waves into estimates of airfoil flutter in the "subtransonic" range of flight Mach numbers. For single-degree-of-freedom pitching motion and for typical section models simulating wing bending and torsion, critical speeds are presented in a manner designed to illustrate the consequences of varying several system parameters. In each case, the shock's role is highlighted by comparative calculations with shock terms removed from the equations of motion.

Some possibly significant conclusions from the investigation may be summarized as follows:

1) The shock's influence on pure pitching instability is markedly unfavorable in the circumstances where this phenomenon is most likely to be encountered. Pure plunging motion, however, experiences added damping due to the shock.

2) The influence may be favorable or unfavorable on the critical speed of flexure-torsion flutter, its direction depending in a complicated way on all system parameters. Unsteady shock effects are often quite pronounced and should not be omitted from flutter calculations. In particular, the phase lag ϕ_s is important even at low reduced frequency.

3) Because of shock weakening near the design point of a supercritical wing, flutter clearance should not be based only on tests close to that point; off-design conditions may be more hazardous.

4) At the high μ characteristic of tests like those of Farmer and Hanson,[1] it is easy to understand the larger changes in critical dynamic pressure due to Mach number, profile shape, and angle of attack. The absolute influence of the shock is quite pronounced there.

5) More attention is needed to understanding and correcting the differences between measured airloads and certain CFD predictions. For example, some small-disturbance CFD codes overpredict the shock phase lag ϕ_s.

6)Despite current deficiencies, it is believed that satisfactory quantitative flutter calculations will become possible only when accurate, three-dimensional CFD codes are available.

It is not claimed that the present approach is more than a qualitative tool for assessing the part that shocks play in transonic aeroelastic stability. The effort is believed justified because well over 25,000 flutter points have already been obtained at a cost of $160 on the Stanford IBM 370/168. This is equivalent to some 7 min of CPU time.

Acknowledgments

This research was supported in part by NASA under Grant NGL-05-020-243 and in part by the Air Force Office of Scientific Research under Grant AFOSR 74-2712. The author is appreciative of valuable discussions and correspondence with M. H. Williams of Princeton University and A. R. Seebass III, of the University of Arizona (now University of Washington). Both these gentlemen supplied extensive unpublished data based on their theoretical research. J. Nathman and L. Lehman, Research Assistants in the Department of Aeronautics & Astronautics at Stanford, helped substantially during early phases of the computer programming. S. Triefenbach made singular contributions to manuscript preparation and typing.

References

[1] Farmer, M.G. and Hanson, P.W., "Comparison of Supercritical and Conventional Wing Flutter Characteristics," *Proceedings AIAA/ASME/SAE 17th Structures, Structural Dynamics and Materials Conference*, King of Prussia, Pa., April 1976, pp. 608-611; see also NASA TM X-72837, May 1976.

[2] Farmer, M.G. and Hanson, P.W., personal communication.

[3] McGrew, J.A., et al., "Supercritical Wing Flutter," AFFDL-TR-78-37, Air Force Flight Dynamics Lab., March 1978.

[4] Erickson, A.L. and Stephenson, J.D., "A Suggested Method of Analyzing for Transonic Flutter of Control Surfaces Based on Available Experimental Evidence," NACA RM A7F30, Dec. 1947.

[5] Erickson, L.L., "Transonic Single-Mode Flutter and Buffet of a Low Aspect Ratio Wing Having a Subsonic Airfoil Shape," NASA TN D-7346, Jan. 1974.

[6] Stevenson, J.R., "Shock-Induced Self-Excited Airfoil Bending Oscillations," Los Angeles Division, Rockwell International, paper presented to Aerospace Flutter & Dynamics Council, Las Vegas, Nev., Oct. 19-20, 1978.

[7] Borland, C.J., personal communication, Boeing Commercial Airplane Co.

[8] Ballhaus, W.F., "Some Recent Progress in Transonic Flow Computations," presented at lecture series in Computational Fluid Dynamics, von Kármán Institute, Belgium, March 15-19, 1976.

[9] Ballhaus, W.F. and Goorjian, P.M., "Computation of Unsteady Transonic Flows by the Indicial Method," AIAA Paper 77-447; also *AIAA Journal*, Vol. 16, Feb. 1978, pp. 117-124.

[10] Rizzetta, D.P., "The Aeroelastic Analysis of a Two-Dimensional Airfoil in Transonic Flow," Air Force Flight Dynamics Lab., AFFDL-TR-77-126, Dec. 1977; see also AFFDL-TM-77-64-FBR, July 1977.

[11] Ballhaus, W.F. and Goorjian, P.M., "Implicit Finite-Difference Computations of Unsteady Transonic Flows about Airfoils," *AIAA Journal*, Vol. 15, Dec. 1977, pp. 1728-1735.

[12] Yang, T.Y., Striz, A.G., and Guruswamy, P., "Flutter Analysis of Two-Dimensional and Two-Degree-of-Freedom Airfoils in Small-Disturbance Unsteady Transonic Flow," Air Force Flight Dynamics Lab., AFFDL-TR-78-202, Dec. 1978 (to be released for publication; draft copy kindly supplied by the authors).

[13] Traci, R.M., Albano, E.D., and Farr, J.L., "Small Disturbance Transonic Flows About Oscillating Airfoils and Planar Wings," Air Force Flight Dynamics Lab., AFFDL-TR-75-100, June 1975.

[14] Baldwin, B.S., MacCormack, R.W., and Deiwert, G.S., "Numerical Techniques for the Solution of the Compressible Navier-Stokes Equations and Implementation of Turbulence Models," NATO Advisory Group for Aeronautical Research and Development, AGARD LSP-73, 1975.

[15] Yates, E.C., Jr., "Modified-Strip-Analysis Method for Predicting Wing Flutter at Subsonic to Hypersonic Speeds," *Journal of Aircraft*, Vol. 3, Jan.-Feb. 1966, pp. 25-29.

[16] Yates, E.C., Jr., personal communication.

[17] Garner, H.C., "A Practical Approach to the Prediction of Oscillatory Pressure Distributions on Wings in Supercritical Flow," Royal Aircraft Establishment, Tech. Rept. 74181, Feb. 1975; see also R.A.E. Tech. Memo Structures 900, Jan. 1977.

[18] Tijdeman, H., "Investigations of the Transonic Flow Around Oscillating Airfoils," Doctoral Dissertation, Technical Univ. of Delft, the Netherlands, Dec. 1977.

[19] Seebass, A.R., et al., "Unsteady Transonic Flow Computations," *Unsteady Aerodynamics*, AGARD Conference Proceedings 227, Sept. 1977.

[20] Williams, M.H., "Unsteady Thin Airfoil Theory for Transonic Flows with Embedded Shocks," Princeton Univ., MAE Rept. 1376, May 1978.

[21] Magnus, R.J., "Computational Research on Inviscid Unsteady Transonic Flow over Airfoils," Office of Naval Research, Rept. CASD/LVP 77-010, Jan. 1977.

[22] Knechtel, E.D., "Experimental Investigation at Transonic Speeds of Pressure Distributions over Wedge and Circular-Arc Airfoil Sections and Evaluation of Perforated-Wall Interference," NASA TN D-15, Aug. 1959.

[23] McDevitt, J.B., Levy, L.L., Jr., and Deiwert, G.S., "Transonic Flow about a Thick Circular-Arc Airfoil," *AIAA Journal*, Vol. 14, May 1976, pp. 606-613.

[24] Montoya, L.C. and Banner, R.D., "F-8 Supercritical Wing Flight Pressure, Boundary-Layer, and Wake Measurements and Comparisons with Wind Tunnel Data," NASA TM X-3544, June 1977.

[25] Harris, C.D. and Bartlett, D.W., "Tabulated Pressure Measurements on a NASA Supercritical Wing Research Airplane Model With and Without Fuselage Area-Rule Additions at Mach 0.25 to 1.00," NASA TM X-2634, 1972.

[26] Kemp, N.H. and Homicz, G., "Approximate Unsteady Thin-Airfoil Theory for Subsonic Flow," *AIAA Journal*, Vol. 14, Aug. 1976, pp. 1083-1089.

[27] Bisplinghoff, R.L., Ashley, H., and Halfman, R.L., *Aeroelasticity*, Addison-Wesley Publishing Co., Reading, Mass., 1955.

[28] van der Vooren, A.I., "The Theodorsen Circulation Function; Aerodynamic Coefficients," *AGARD Manual on Aeroelasticity*, W.P. Jones, ed., published by NATO Advisory Group on Aeronautical Research and Development, Vol. VI, Jan. 1964.

[29] Theodorsen, T., "General Theory of Aerodynamic Instability and the Mechanism of Flutter," NACA Rept. 496, 1935.

[30] Runyan, H.L., "Single-degree-of-freedom Flutter Calculations for a Wing in Subsonic Potential Flow and Comparison with an Experiment," NACA TN 2396, 1951.

[31] Runyan, H.L., personal conversation.

[32] Garrick, I.E., "Bending-Torsion Flutter Calculations Modified by Subsonic Compressibility Corrections," NACA Rept. 836, 1946.

[33] Fung, K-Y., Yu, N.J., and Seebass, A.R., "Small Unsteady Perturbations in Transonic Flows," *AIAA Journal*, Vol. 16, Aug. 1978, pp. 815-822.

[34] Seebass, A.R., personal communication.